PERGAMON

International Journal of Heat and Mass Transfer 42 (1999) 573–579

International Journal of HEAT and MASS TRANSFER

Numerical simulation of a 2-D crystal growth problem in vertical Bridgman–Stockbarger furnace: latent heat effect and crystal–melt interface morphology

D. Morvan*, M. El Ganaoui, P. Bontoux

Institut de Recherche sur les Phénomènes Hors Équilibre, Unité Mixte de Recherche 6594 CNRS Universités d'Aix-Marseille 1 & 2, UNIMECA 60 rue Joliot Curie, Technopôle de Château Gombert, 13453 Marseille cedex 13, France

Received 29 October 1996; in final form 31 March 1998

Abstract

The influence of latent heat and natural convection upon the melt–crystal interface in a vertical Bridgman–Stockbarger crystal growth system is studied by numerical simulation. The temperature and velocity field are computed using an average technique which consists of representing the solid–liquid mixture as a single continuum medium. The physical properties of the equivalent medium are evaluated from average values which characterize each phase present in the system. The numerical resolution is performed using a finite volume method including a high-order upwind scheme and PISO algorithm for the pressure–velocity coupling. The numerical results show the effects of latent heat and gravity magnitude upon the flow pattern in the melt. The consequences upon the melt–crystal interface are also analyzed.

Nomenclature

c specific heat
d crystal diameter
F volume force
f mass fraction
g volume fraction or gravity acceleration
h enthalpy
h_f solid–liquid phase change latent heat
K permeability
K_0 permeability in Carman–Kozeny equation
k conductivity
p pressure (isotropic stress component)
Pe Peclet number
Pr Prandtl number
Ra Rayleigh number
Ste Stefan number
S source term
T temperature
T_f solid–liquid phase change temperature
U_s crystal growth velocity
v_i velocity vector components
x_i Cartesian coordinate.

Greek symbols
β thermal coefficient of volume expansion
μ dynamic viscosity
ρ density
ϕ general scalar quantity.

Superscripts and subscripts
f melt conditions
l liquid phase
s solid phase
ϕ solid or liquid phase.

1. Introduction

To increase the dimensions (diameter) of single crystals (used in electronic components industry) produced using growth techniques, it is necessary to understand more accurately physical mechanisms associated with solidification problems. For example, directional solidification processes such as crystal growth from the melt

* Corresponding author

0017–9310/98 $19.00
PII: S0017–9310(98)00141–0

(Czochralski, floating-zone, Bridgman–Stockbarger ...), are greatly affected by physical and chemical transport phenomena inside the liquid phase and near the melt–crystal interface [1]. The formation of a single crystal results from carefully controlled solid–liquid phase change. The buoyant flow induced by temperature gradients in the melt represents the major contribution for heat and mass transfer and affects very significantly the resulting dopant distribution in the crystal [2]. The relation between microscopic variations in the structure of the crystal (crystallographic perfection of the lattice) and macroscopic processing variables are largely unknown. Direct numerical simulations allows to study the consequences induced by various physical parameters such as material properties or experimental conditions. The crystal growth systems can be classified in two categories of confined (vertical Bridgman–Stockbarger, gradient freeze methods) and meniscus-defined (Czochralski, floating zone methods). The most popular growth method in industry is the Czochralski technique. This method allows to produce in industrial environment large diameter single crystals but sometimes it is more suitable to use confined melt growth method. This method permits for example to produce in better conditions, exotic alloy materials with an accurate control of the stoichiometry. In confined growth techniques, the material is loaded into an ampoule, melted and resolidified by varying the temperature field induced at the surface of the ampoule by the heat sources distributed in the furnace. Another advantage of this method is to obtain a better control of axial temperature gradients which are needed to produce crystals with low dislocation densities.

The crystal growth system studied in the present article is a vertical Bridgman–Stockbarger furnace. The heating apparatus includes a cold and a hot isothermal zone. The connection between these two regions is ensured by an adiabatic zone where the solid–liquid phase change occurs (see Fig. 1). The initially poly-crystal material is melted and placed in the ampoule which is translated inside the furnace at very slow scanning velocity (1–5 μ/s). The accurate control of processing conditions (temperature gradient, scanning velocity ...) allows the transformation of the material to a single-crystal small bar. The aim of this study is to analyze the various flow patterns in the melt for different gravity magnitudes and temperature range in the furnace. We have also studied the consequences upon the crystal–melt interface.

2. Mathematical formulation and numerical resolution

To solve the present fusion–solidification problem, we have chosen a single domain method which consists of reducing the multicomponent and multiphase medium as a single continuum medium using an average technique.

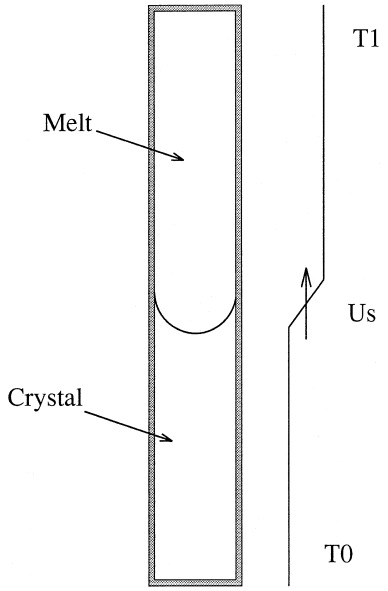

Fig. 1. Bridgman–Stockbarger crystal growth technique (ampoule geometry and temperature boundary conditions).

In this case the solid–liquid interaction terms are implicitly included through the definition of new average variables. Compared to standard multi-domain approach [3], this method does not need boundary conditions at the solid–liquid interface. This method can be applied with success, to complex solid–liquid phase change problems such as those encountered during dendritic growth of alloy materials [4]. The source terms which appear in the average conservation equations (mass, energy, momentum) represent the interaction between the solid and liquid phases (latent heat, friction ...). In the momentum equations, the solid–liquid interaction force is represented with a Darcian type source term which supposes that the melt flow in the phase change zone is similar to an incompressible viscous flow in a porous medium.

For isothermal solid–liquid phase change problems (pure or eutectic alloy material) the two methods (single and multi-domain) produce similar results, with a good agreement with the analytical solutions obtained for simple configurations [5] but also with experimental observations for more complex situations [6]. Using average approach, the average mass, energy and momentum conservation equations can be written as follows [7]:

$$\frac{\partial}{\partial t}(\rho)+\frac{\partial}{\partial x_j}(\rho v_j)=0 \tag{1}$$

$$\frac{\partial}{\partial t}(\rho v_i)+\frac{\partial}{\partial x_j}(\rho v_j v_i)=-\frac{\partial p}{\partial x_i}+\frac{\partial}{\partial x_j}\left(\mu_l\frac{\rho}{\rho_l}\frac{\partial v_i}{\partial x_j}\right)+\rho F_i+F_i^{\mathrm{sl}} \tag{2}$$

$$\frac{\partial}{\partial t}(\rho h)+\frac{\partial}{\partial x_j}(\rho v_j h)=\frac{\partial}{\partial x_j}\left(\frac{k}{c_s}\frac{\partial h_s}{\partial x_j}\right)-\frac{\partial}{\partial x_j}\left(\rho(h_l-h)(v_j-v_j^s)\right). \tag{3}$$

The average density, velocity vector components, enthalpy and thermal conductivity are defined as follows:

$$\rho = g_s\rho_s+(1-g_s)\rho l \tag{4}$$

$$v_i = f_s v_i^s+(1-f_s)v_i^l \tag{5}$$

$$h = f_s h_s+(1-f_s)h_l \tag{6}$$

$$k = g_s k_s+(1-g_s)k_l \tag{7}$$

If we suppose that the specific heats for the liquid and the solid phases are constant, the enthalpies for each phase (h_s and h_l) varie linearly with the temperature:

$$h_s = c_s T \tag{8}$$

$$h_l = c_l T+[(c_s-c_l)T_f+h_f] \tag{9}$$

where h_f and T_f represent respectively, the solid–liquid phase change latent heat evaluated at the reference temperature T_f, which could be the melt temperature for a pure material or the eutectic temperature for binary alloy material. To construct the average momentum equation, we have also supposed that the stress in the solid phase can be neglected and the diphasic zone was saturated ($g_s+g_l=1$). The requirements of mixture saturation and a stress-free solid phase need the additional assumption that the densities of the solid and liquid phases must be equal ($\rho_s=\rho_l$), without which a void could form ($\rho_s>\rho_l$) or the constraint of a stress-free solid could not be enforced ($\rho_s<\rho_l$) [8]. In this case volume (g_s) and mass fraction (f_s) for the solid phase are identical and can be evaluated directly from enthalpy field.

The modelling of liquid–solid interaction forces F_i^{sl} could be represented in two different manners [9]:

—For systems in which there is no relative motion between melt and solid (e.g. waxes and glasses), one can represent the phase change region as a mushy fluid with a viscosity function based on local volume solid fraction g_s (with a sharp increase as the temperature is inferior to the liquidus temperature). In this case the solid–liquid interaction force is $F_i^{sl}=0$.

—For systems in which the motions of the liquid and solid phases are distinct (columnar dendritic growth, e.g. metals), the melt flow in the mushy zone is represented as a viscous flow in a porous medium with a permeability function based on g_s. In this case the solid–liquid interaction force is evaluated from Darcy law:

$$F_i^{sl} = -\frac{\mu_l}{K}\frac{\rho}{\rho_l}(v_i-v_i^s). \tag{10}$$

The permeability which appears in this last expression is defined as a function of the local liquid volume fraction as it is often used for viscous flows in porous media (Carman–Kozeny relation):

$$K = K_0\left[\frac{(1-g_s)^3}{g_s^2}\right] \tag{11}$$

K_0 depends on the solidification microstructures, for the present calculation we have fixed $K_0 = 5\ 10^{-11}$ which corresponds to microstructures dimensions of 100 μm [10].

This last model is the most appropriate approximation of solid–liquid interaction during most of fusion–solidification problems until the solid volume fraction $g_s>0.5$. When $g_s<0.5$ the Carman–Kozeny relation induces an over estimation of the solid–liquid friction which supress the effects of the other volume force such as buoyancy force. This default could be corrected using an hybrid model which combines the two previous approaches, a variable viscosity and a variable permeability [11]:

$$\mu_l = \mu_l^0\left(\frac{A_\mu}{A_\mu-Fg_s}\right)^2 \tag{12}$$

$$K = GK_0\left[\frac{(1-g_s)^3}{g_s^2}\right] \quad (A_\mu=0.4). \tag{13}$$

The introduction of ad-hoc functions F, G must reduce the effects of an excessive dumping of the flow in the mushy zone due to the action of the Darcy force. The shape of these functions has been chosen according to the theory of rheology of suspensions:

$$F = 0.5-\frac{1}{\pi}\arctan[100(g_s-g_s^{crit})] \tag{14}$$

$$G = \left[0.5+\frac{1}{\pi}\arctan[100(g_s-g_s^{crit})]\right]^{-4}. \tag{15}$$

The critical value for the solid volume fraction g_s^{crit} which separates the two solid–liquid phase change modelling is fixed as $g_s^{crit}=0.5$, which represents the limit of validity of the Carman–Kozeny relation for viscous flows in porous media.

The resulting set of partial differential equations is solved using a finite-volume method [12, 13]. The time integration is performed using a first order Euler implicit Euler scheme. To avoid numerical diffusion, the interface fluxes are approximated using an Ultra-Sharp scheme which combined a centered approximation for the diffusive part and a high order Upwind scheme for the convective part. To guarantee none-oscillatory results this approach is completed with an universal flux limiter [14].

The resulting set of algebraic equations is solved with a PISO algorithm [15] which exhibits superior performance (computational effort, good convergence and consistent

behaviour) than other segregated algorithms such as SIMPLE-like algorithms. The convergence criteria to stop iterative procedure are defined from the ratio between the residual at the kth iteration and at initial value (it must be less than 0.05 for pressure and 0.2 for other transported variables). To complete convergence criteria we have also imposed that the Euclidean norm of the residual in the whole computational domain must be less than 10^{-6}.

3. Numerical results and discussion

The geometry of the computational domain is rectangular with a length/width shape ratio equal to 10. The problem is solved in a fixed referential with regard to the ampoule, therefore the cooling induced by the furnace is represented with a time dependent temperature profile along the lateral boundary of the ampoule characterized with a scanning velocity U_s. The temperature profile along lateral boundary is composed by two isothermal zones (hot temperature T_1 and cold temperature T_0) linked by an adiabatic plug zone with a width equal to two times the ampoule diameter (Fig. 1) and animated with a constant translation velocity U_s. The boundary conditions for the velocity vector components are $v_j = 0$ on the ampoule wall. Excepting on the adiabatic region, the temperature is fixed on the ampoule walls ($T = T_0$ or $T = T_1$, respectively, in the cold and hot region).

In order to reduce the number of physical parameters, the transport equations (1)–(3) are transformed in dimensionless form using the following reference scales:

—length: crystal diameter d
—temperature (maximum temperature variation in the furnace): $\Delta T = T_1 - T_0$
—density, specific heat and conductivity: ρ_l, c_s and k_l
—velocity: $U = kl/\rho c_s d$
—enthalpy: $c_s \Delta T$

In this case the physical system is completely defined from four dimensionless parameters:

$$\text{Rayleigh number: } Ra = \frac{g\beta c_s \Delta T \rho^2 d^3}{k\mu}$$

$$\text{Prandtl number: } Pr = \frac{\mu_l c_s}{k_l} \tag{16}$$

$$\text{Stefan number: } Ste = \frac{c_s \Delta T}{h_f}$$

$$\text{Peclet number: } Pe = \frac{U_s}{U} \tag{17}$$

where U_s is the crystal growth (scanning) velocity. The calculations have been performed for a 28×200 mesh grid. Previous numerical results [16] have shown that a boundary layer regime can develop along the vertical walls of the ampoule when the convective transport increase in the melt. Therefore to obtain an adequate accuracy near the ampoule wall, the mesh is locally refined along the vertical boundaries. The tested values for the dimensionless physical parameters are evaluated from experimental conditions of a crystal growth operation for a semiconductor material such as gallium-doped germanium (Ga–Ge) [17], the corresponding values for Pr and Pe are 10^{-2} and 5×10^{-3}, respectively. The solid–liquid phase change is assumed to occur between a solidus (T_s) and a liquidus (T_l) temperature equal to 0.4 and 0.6 [dimensionless values defined as $(T - T_0)/(T_1 - T_0)$] which correspond for example to a 1.25% gallium-doped germanium with a temperature variation in the furnace of 250 K and microgravity conditions of 2×10^{-4}–2×10^{-2} g.

The numerical results presented on Fig. 2 show the evolution of the velocity field obtained for $Ra = 10^3$ and $Ste^{-1} = 0$ at different times during crystal growth process. In this case, the flow pattern is symmetrical and composed with four vortices. Excepting at the end of the solidification, the melt flow near the crystal–melt interface (which represents the most important contribution for the crystal growth process) is not affected by the continuous reduction of the melt region. During all the solidification the crystal–melt interface (represented here by the solidus isothermal curve) remains flat. The results presented on Fig. 3 show the velocity field obtained at intermediate time for two values of the Rayleigh number ($Ra = 10^3$, 10^5) and three values of the Stefan number ($Ste^{-1} = 0$, 5, 10). The increase of latent heat effects induces two main phenomena, the crystal–melt interface becomes curved and new recirculating cells appear in the melt region. For this set of physical parameters the solution always converges to a steady state and the flow pattern is symmetrical. The increase of latent heat represents a supplementary energy which must be extract to the material before solidification. This modification of the phase-change conditions is illustrated by an increase of the melt region in front of the solidification interface where the transverse temperature gradient can be very important inducing high buoyant recirculating flow. For $Ste^{-1} = 5$ and $Ste^{-1} = 10$ we can observe respectively six and heigh recirculating cells in the melt. The increase of gravity magnitude seems to have no effect upon the shape of solidification front.

4. Conclusion

A finite volume discretization model using average technique has been presented for the resolution of a crystal growth problem. Numerical results have shown a great influence on the latent heat upon the shape of the phase-change front and the flow of the melted material in this region. The gravity magnitude represented by the

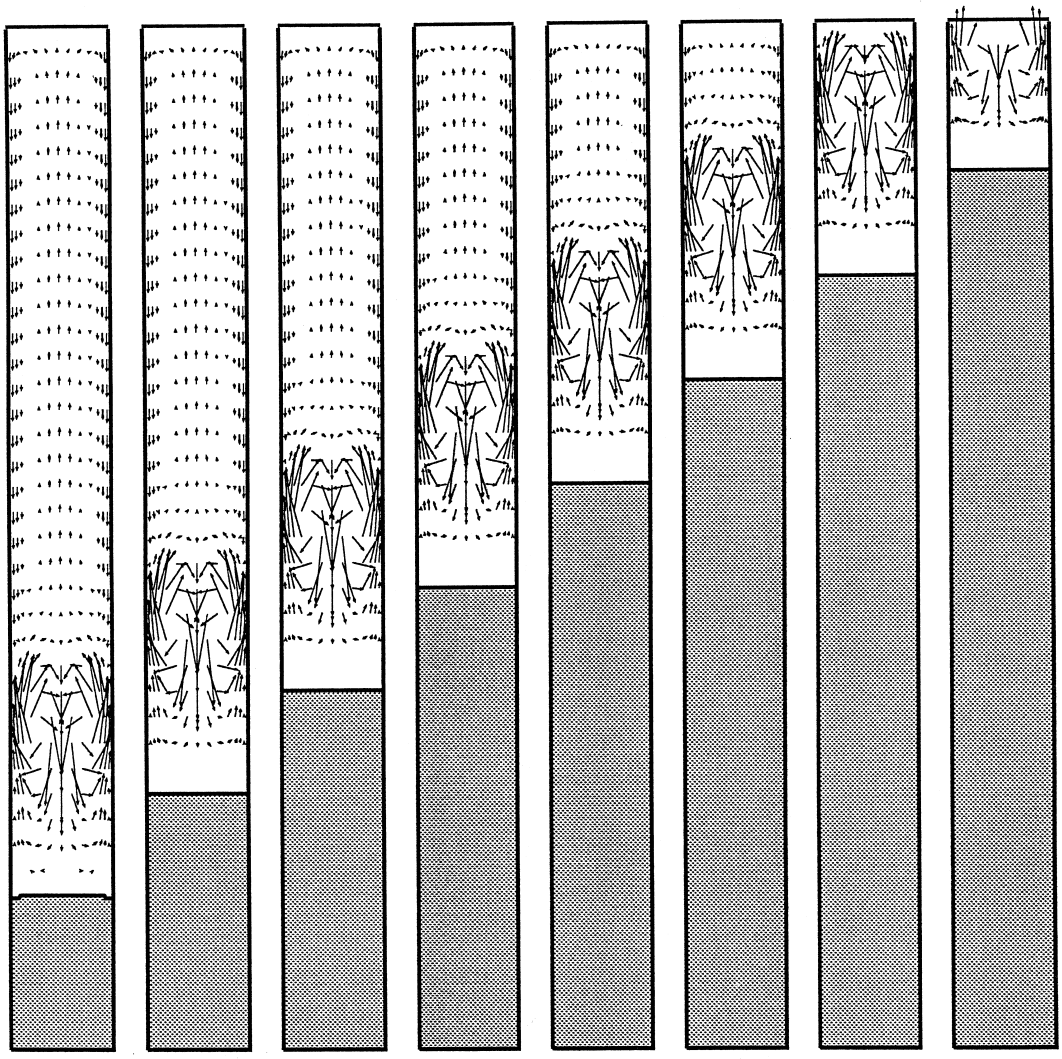

Fig. 2. Flow pattern in the melt during a crystal growth process for $Ra = 10^3$ and $Ste^{-1} = 0$.

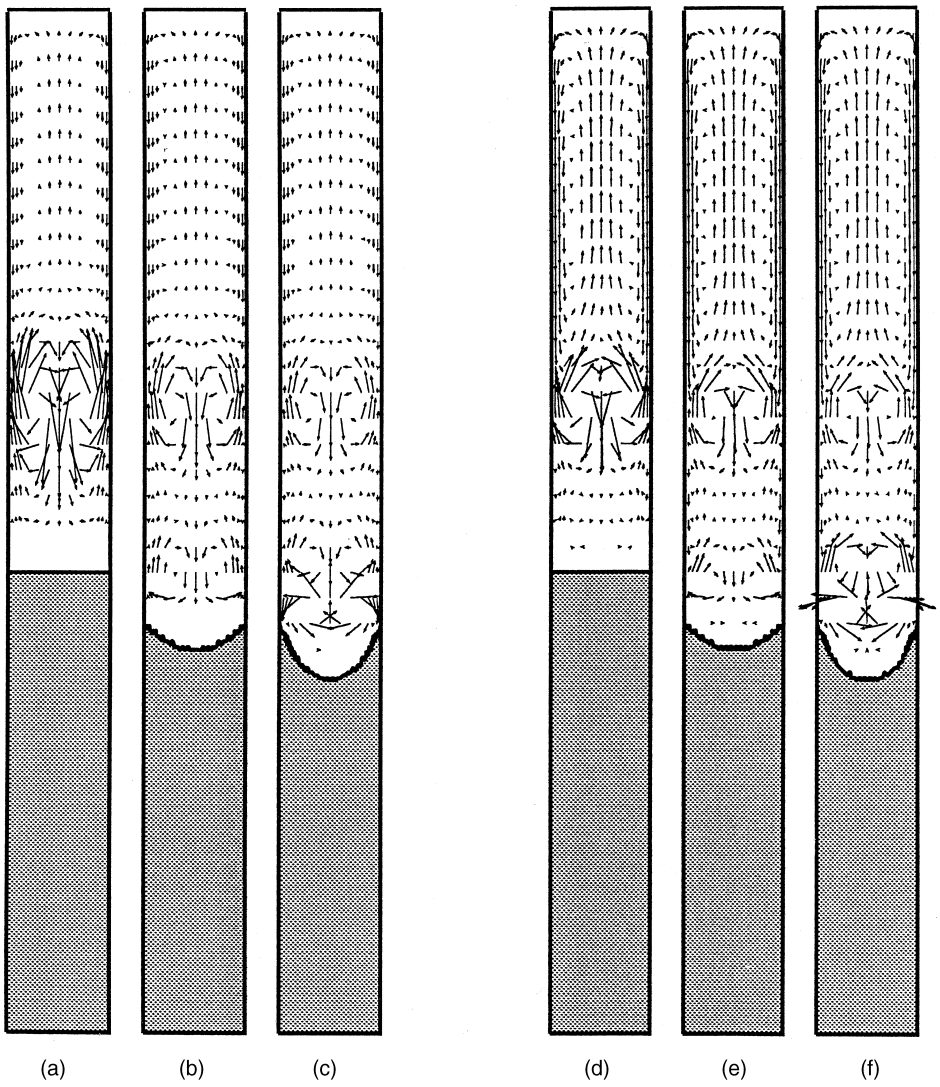

Fig. 3. Flow pattern in the melt during a crystal growth process for $Ste^{-1} = 0$, 5, 10 and $Ra = 10^3$ (a–c), $Ra = 10^5$ (d–f), $U_{max} = 0.13$ (a), 0.06 (b), 0.075 (c), 2.95 (d), 2.345 (e, f) (dimensionless value).

Rayleigh number seems to have no effect upon the shape and the propagation of the melt–crystal front. The deformation of this phase–change interface seems to be essentially affected by the latent heat to sensible heat ratio and the dimension of the adiabatic zone along the wall of the ampoule.

Before their generalization these results must be confirmed for larger selection of the physical parameters, for example for larger values of the crystal growth velocity represented by the Peclet number and other configuration of temperature boundary conditions along the lateral face of the ampoule, including for example the effects of heat transfer through the ampoule wall.

References

[1] S. Ostrach, Low-gravity fluid flows, Ann. Rev. Fluid Mech 14 (1982) 313–345.
[2] R.A. Brown, Theory of transport processes in single growth from the melt, AIChE Journal 34 (6) (1988) 881–911.
[3] H. Rieger, U. Projahn, M. Bareiss, H. Beer, Heat transfer

during melting inside a horizontal tube, J. Heat Transfer Trans. ASME 105 (5) (1983) 226–234.
[4] D.G. Neilson, F.P. Incropera, Unidirectional solidification of a binary alloy and the effects of induced fluid motion, Int. J. Heat Mass Transfer 34 (7) (1991) 1717–1732.
[5] V. Voller, M. Cross, Accurate solutions of moving boundary problems using the enthalpy method, Int. J. Heat Mass Transfer 24 (1981) 545–556.
[6] D.G. Neilson, F.P. Incropera, W.D. Bennon, Numerical simulation of solidification in a horizontal cylindrical annulus charged with an aqueous salt solution, Int. J. Heat Mass Transfer 33 (2) (1990) 367–380.
[7] W.D. Bennon, F.P. Incropera, A continuum model for momentum, heat and species transport in binary solid–liquid phase change systems: 1 model formulation, Int. J. Heat Mass Transfer 30 (10) (1987) 2161–2170.
[8] F.P. Incropera, H.H. Engel, W.D. Bennon, Numerical analysis of binary solid–liquid phase change with buoyancy and surface tension driven convection, Numerical Heat Transfer, Part A 16 (1989) 407–427.
[9] V. Voller, A.D. Brent, The modelling of heat, mass and solute transport in solidification systems, Int. J. Heat Mass Transfer 32 (9) (1989) 1719–1731.
[10] C. Beckermann, R. Viskanta, Double-diffusive convection during dendritic solidification of a binary mixture, Physico-Chemical Hydrodynamics 10 (2) (1988) 195–213.
[11] C.M. Oldenburg, F.J. Spera, Hybrid model for solidification and convection, Numerical Heat Transfer, Part B 21 (1992) 217–229.
[12] S.V. Patankar, Numerical Heat Transfer and Fluid Flow, Hemisphere Publishing, New York, 1980.
[13] J.P. Van Doormaal, G.D. Raithby, Enhancements of the simple method for predicting incompressible fluid flow, Numerical Heat Transfer 7 (1984) 147–163.
[14] W.J. Minkowicz, (Ed), Handbook of Numerical Heat Transfer, Chap. 9, p. 347–378, Springer-Verlag, Berlin Heidelberg, 1988.
[15] D.S. Jang, R. Jetli, S. Acharya, Comparison of the piso, simpler and simplec algoritms for the treatment of the pressure–velocity coupling in steady flow problems, Numerical Heat Transfer 10 (1986) 209–228.
[16] P.M. Adornato, R.A. Brown, Convection and segregation in directional solidification of dilute and non-dilute binary alloys: effects of ampoule and furnace design, J. Crystal Growth 80 (1987) 155–190.
[17] J. Chang, R.A. Brown, Radial segregation induced by natural convection and melt–solid interface shape in vertical Bridgman growth, J. Crystal Growth 63 (1983) 343–364.